imaging of myocardial oxygenation induced by endothelium dependent and independent vasodilation. Signal intensities correlate with coronary venous SaO2 and T2* of the myocardium. Further studies should address its feasibility in clinical settings.

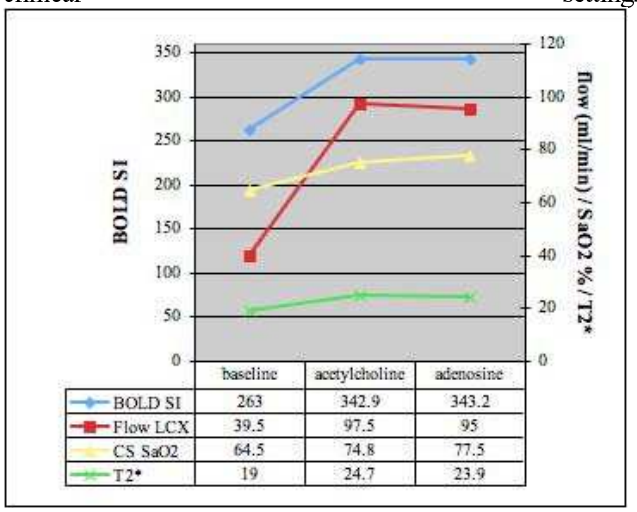

	baseline	acetylcholine	adenosine
BOLD SI	263	342.9	343.2
Flow LCX	39.5	97.5	95
CS SaO2	64.5	74.8	77.5
T2*	19	24.7	23.9

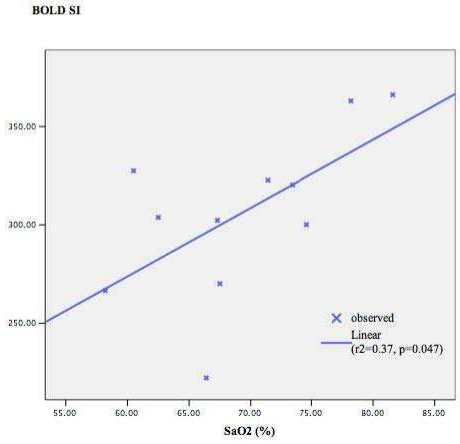

2133. EFFECT OF THE BOLUS SIZE ON THE QUANTIFICATION OF MYOCARDIAL PERFUSION USING MRI

Marko Ivancevic, PhD, Jean-Luc Daire, PhD, Michel Kocher, PhD, Alberto Righetti, MD, Dominique Didier, MD, Jean-Paul Vallée, MD, PhD. Geneva University Hospital, Geneva, Switzerland.

Introduction: A limitation of MRI for cardiac perfusion on routine clinical MR scanners is the trade-off between the temporal resolution and spatial coverage. Assuming that a higher contrast media dose and a slower injection rate allow lower sampling rate without a significant loss of precision in an one compartmental model, we performed a simulation study to compare two contrast injection strategies (wide and narrow bolus). The validity of the protocol was then demonstrated in patients with a history of myocardial infarction, using 201-Tl SPECT imaging as reference.

Methods: The myocardial perfusion is quantified using the one compartment model described by: dCmyo(t)/dt=K1Cart(t) - K2Cmyo(t) where Cart(t) and Cmyo(t) are the arterial and myocardial signal intensity time curves respectively, K1 the perfusion index related to the first order transfer constant from the LV blood to the myocardium and the ratio K1/K2 the fractional distribution volume of the contrast media. Simulation study: to evaluate the effect of the bolus shape on the model, two arterial input functions (AIF), narrow (0.035 mmol/kg at 5 cc/sec) and wide (0.08 mmol/kg at 0.5 cc/sec) were derived from real data and used as input stimuli. Using a constant value for K1 and K2, Cmyo curves have been simulated by the discrete transfer function of the one compartment model derived from the Laplace transform. The output error (OE) method was used as a system identification method to estimate K1 and K2. Finally, estimated values of K1 and K2 are described for different noise indices (the standard deviation of a zero mean Gaussian process varies from 0 to 10%) and different under-sampling strategies. Bias and standard deviation of fitted K1 and K2 values were described in each case as well as the Bode diagram. Clinical study: The validity of the protocol was then demonstrated in 12 patients with a history of myocardial infarction, using 201-Tl SPECT imaging as reference. The MR perfusion sequence was a T1 weighted FGRE sequence with eight slices (4 short-axis, and 4 long-axis) acquired during three to six cardiac cycles, depending on patient's heart rate. the average inter-image delay was 4 seconds (±0.5). A bolus of 0.08 mmol/kg Gd-DTPA was injected in a brachial vein at 0.5 ml/s injection rate. Standard one compartment model analysis was then applied.

Results: Simulation study: the Bode diagram showed a similar behaviour of the narrow and wide AIF around the cut-off frequency and indicating that both bolus shapes are adapted to this one compartment model. No significant difference in bias and standard deviation were observed with the identification process between the two shapes. Under-sampled curves introduce an increase of standard deviation of K1 and K2 but with a lower bias for the broad AIF. For typical noise encountered in patient data (around 1%), the standard deviation and biais remain within acceptable limits (< 5 %).

In the clinical study, the wide AIF protocol was able to differentiate between normal and abnormal thallium sectors. A decrease in the perfusion values measured by MRI in the infarcted regions was observed (k1= 0.27 ± 0.21 ml/min/g compared to 0.4 ± 0.21 ml/min/g in normal, p 0.8).

Conclusions: The technique presented here overcomes the spatial limitation of cardiac MR perfusion assessment by allowing for reduced temporal acquisition rate without significant loss in accuracy for the perfusion quantification.

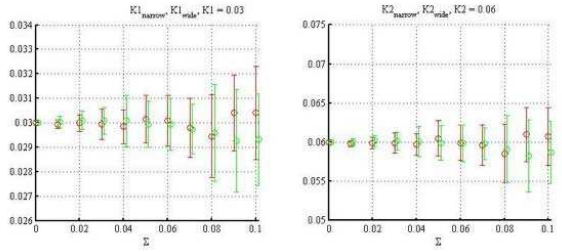

Figure 2: Fitted k1 and k2 values versus noise for the narrow and wide AIF. In this case, K1 was fixed to 0.03 and K2 = 0.06. Similar biais and deviation standard was observed for both AIF . Each point ± s.d is the result of 80 iterations.

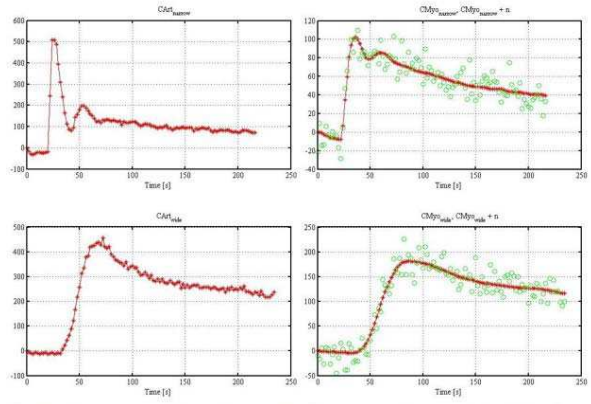

Figure 1: Narrow and wide arterial input function measured from real data (left column) and the corresponding myocardial simulated responses with (circles in the right column) and without (diamonds in the right columns) added noise.

2134. VALIDATION OF THE SPIRAL FOURIER VELOCITY ENCODING METHOD

Joao L. A. Carvalho, Jon F. Nielsen, Krishna S. Nayak. University of Southern California, Los Angeles, CA, USA.

Introduction: Phase-contrast (PC) is the current "gold standard" for MR flow quantitation, despite suffering from partial volume effects. Fourier velocity encoding (FVE) resolves the distribution of velocities within each voxel, allowing larger voxels to be used. In 1995, Frayne et al. [1] proposed 2DFT FVE as a method for non-invasively measuring fluid shear rate and hence vascular wall shear stress, an important factor implicated in atherogenesis. Although the scan-time of this method was prohibitively long, the recently introduced spiral FVE method [2] shows promise as it is substantially faster. In this work, we provide an initial validation of spiral FVE in a carotid artery flow phantom, using high-resolution PC as the gold standard.

Theory: The spiral FVE method acquires a stack-of-spirals in k_x,k_y,k_v space [2], where k_v is the Fourier variable associated with the velocity distribution. Truncation in k-space follows a cylindrical shape, i.e. circular along k_x,k_y (with diameter $1/xy_{res}$), and rectangular along k_v (with width $1/v_{res}$). The associated object-domain blurring can be modeled as convolution of $m(x,y,v)$ with $jinc(sqrt(x^2+y^2)/xy_{res})$ and $sinc(v/v_{res})$.

Methods: Experiments were performed on a GE Signa Excite HD 3T scanner with a pulsatile carotid flow phantom (Phantoms by Design, Inc.). A slice perpendicular to the carotid bifurcation was prescribed, and through-plane velocities were measured. A gradient-echo 2DFT phase-contrast sequence (0.33 mm resolution, 10 NEX) was used as a gold standard reference. Spiral FVE data with 3 mm resolution was obtained from the same scan plane. Both PC and FVE acquisitions were prospectively gated. The total scan time was 22 minutes for PC, and 24 seconds for FVE. A simulated FVE dataset was derived from PC using the convolution model described above. For each temporal phase, the images $m(x,y)$ and $pc(x,y)$ (magnitude and phase difference, respectively) were used as follows: $fve(x,y,v) = [\, m(x,y) \,.\, sinc\,(v\text{-}pc(x,y))/v_{res}\,] * jinc(sqrt(x^2+y^2)/xy_{res})$ Spatial registration between PC-derived and measured FVE data was performed by visual inspection.

Results: For reference, magnitude and phase-difference images obtained from the first temporal phase of the phase-contrast data are shown in Fig. 1. Simulated and measured time-velocity FVE distributions from representative voxels (circles in Fig. 1) are shown in Fig. 2. Despite differences in temporal resolution, SNR, TR, flip angle and slice profile, good agreement was observed between simulated and measured FVE distributions. These results suggest that spiral FVE is capable of providing velocity histograms equivalent to those obtained with high-resolution 2DFT phase-contrast, in considerably shorter scan time.

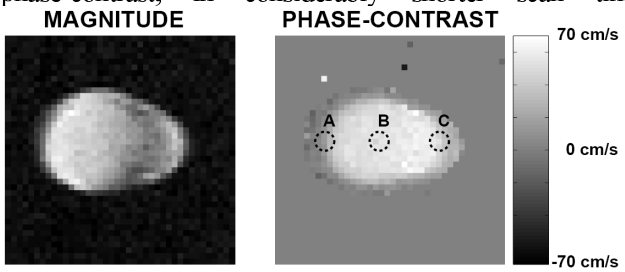

Fig. 1: Magnitude and phase-difference images obtained from the first temporal phase of the PC data.

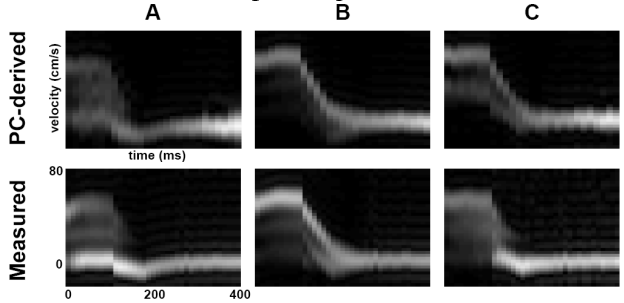

Fig. 2: PC-derived (top row) and spiral FVE (bottom row)